Luminex®

complexity simplified.

Innovative, Intuitive, Flexible

Amnis® and Guava® Flow Cytometry Systems Are Now Part of Luminex.

Learn More

Cytometry PART A
ISAC
Journal of Quantitative Cell Science

MIFlowCyt

Morpho-Rheological Fingerprinting of Rod Photoreceptors Using Real-Time Deformability Cytometry

Tiago Santos-Ferreira,[1] Maik Herbig,[2] Oliver Otto,[2,5] Madalena Carido,[1] Mike O. Karl,[1,3] Stylianos Michalakis,[4] Jochen Guck,[2] Marius Ader[1*]

[1]CRTD/Center for Regenerative Therapies Dresden, Center for Molecular and Cellular Bioengineering, Technische Universität Dresden, Dresden, Germany

[2]Biotechnology Center, Center for Molecular and Cellular Bioengineering, Technische Universität Dresden, Dresden, Germany

[3]German Center for Neurodegenerative Diseases (DZNE), Dresden, Germany

[4]Center for Integrated Protein Science Munich (CiPSM), Department of Pharmacy—Center for Drug Research, Ludwig-Maximilians-Universität München, Munich, Germany

[5]Centre for Innovation Competence: Humoral Immune Reactions in Cardiovascular Diseases (HIKE), University of Greifswald, Greifswald, Germany

Received 12 March 2019; Revised 30 April 2019; Accepted 6 May 2019

Grant sponsor: Alexander von Humboldt-Stiftung; Grant sponsor: Bundesministerium für Bildung und Forschung (ZIK HIKE); Grant sponsor: Deutsche Forschungsgemeinschaft, Grant numbers: SPP2127 GU612/5-1, KA 2794/5-1, AD375/3-1, AD375/7-1, EXC68, FZT111; Grant sponsor: ProRetina Stiftung; Grant sponsor: Helmholtz-Gemeinschaft Deutscher Forschungszentren, Grant numbers: DZNE, Ex-Net0007

Additional Supporting Information may be found in the online version of this article.

*Correspondence to: Dr. Marius Ader, CRTD/Center for Regenerative Therapies Dresden, Technische Universität Dresden, Fetscherstrasse 105, 01307 Dresden, Germany Email: marius.ader@tu-dresden.de

Tiago Santos-Ferreira and Maik Herbig equally contributed to this work.
Jochen Guck shared co-senior authorship.
Present address of Tiago Santos-Ferreira: Roche Innovation Center Basel, F. Hoffman-La Roche Ltd., Grenzachterstrasse 124, Basel 4070, Switzerland.

Published online in Wiley Online Library (wileyonlinelibrary.com)

DOI: 10.1002/cyto.a.23798

Abstract

Distinct cell-types within the retina are mainly specified by morphological and molecular parameters, however, physical properties are increasingly recognized as a valuable tool to characterize and distinguish cells in diverse tissues. High-throughput analysis of morpho-rheological features has recently been introduced using real-time deformability cytometry (RT-DC) providing new insights into the properties of different cell-types. Rod photoreceptors represent the main light sensing cells in the mouse retina that during development forms apically the densely packed outer nuclear layer. Currently, enrichment and isolation of photoreceptors from retinal primary tissue or pluripotent stem cell-derived organoids for analysis, molecular profiling, or transplantation is achieved using flow cytometry or magnetic activated cell sorting approaches. However, such purification methods require genetic modification or identification of cell surface binding antibody panels. Using primary retina and embryonic stem cell-derived retinal organoids, we characterized the inherent morpho-mechanical properties of mouse rod photoreceptors during development based on RT-DC. We demonstrate that rods become smaller and more compliant throughout development and that these features are suitable to distinguish rods within heterogenous retinal tissues. Hence, physical properties should be considered as additional factors that might affect photoreceptor differentiation and retinal development besides representing potential parameters for label-free sorting of photoreceptors. © 2019 The Authors. *Cytometry Part A* published by Wiley Periodicals, Inc. on behalf of International Society for Advancement of Cytometry.

Key terms

morpho-mechanical properties; retina; photoreceptor; embryonic stem cell

PHOTORECEPTORS represent the main light-sensing cells in the vertebrate retina providing object recognition and vision. Extensive knowledge has been gained over the last decades regarding photoreceptor morphology, differentiation, maturation, and function including in depth molecular expression and ultra-structural analysis providing insights into cell lineage and development at the retinal tissue as well as cellular level (1). However, physical properties of cells are more and more recognized as essential parameters in cell behavior, differentiation, migration, and function, and additionally offer the possibility to develop label-free isolation strategies (2,3). While molecular, biochemical, and genetic factors affecting photoreceptors have been widely assessed, knowledge about the morpho-rheological properties of photoreceptors are limited if not absent.

For most research studies, photoreceptors are isolated from primary retinal tissue—mainly from the mouse, but also from other vertebrate species including humans, however, restricted by limited tissue availability. Recent technology improvements now allow the generation of high amounts of photoreceptors within retinal organoids derived from expandable cell sources such as human/mouse (h/m) embryonic stem cells (ESC) (4–9) or induced pluripotent stem cells (iPSC) (10–14).

in vivo and in vitro generated retinal tissues are composed of heterogenous cell populations and for analysis and/or therapy development, several sorting technologies have been established to isolate and enrich photoreceptors including flow cytometry (e.g., fluorescence-activated cell sorting [FACS] (15–18), immunopanning (19) or magnetic-activated cell sorting [MACS] (20–24)). FACS requires the use of either a fluorescent protein and thus genetic modification of target cells or/and antibodies binding to photoreceptor-specific antigens. A similar principle applies to MACS where an antibody is conjugated to a magnetic bead that allows the separation of labeled cells by magnetic force. Cluster of differentiation (CD) 73 has been identified as a cell surface marker present on rods and absent on other cell types of the mouse retina (25). Indeed, CD73 has been used to purify rods from primary embryonic and postnatal retinas (20–22), as well as mESC-derived retinal organoids by MACS technology for characterization and transplantation purposes (23). Although CD73 alone is sufficient to enrich rod photoreceptors, it can also be combined with other antibodies for more specific, ontogenetic-defined sorting. A photoreceptor-specific antibody panel ($CD73^+/CD24^+/CD133^+/CD47^+/CD15^-$) was elaborated to enrich transplantation competent mESC-derived rods by FACS (26). Recently, it was reported that CD73 is also expressed in human ESC- and iPSC-derived photoreceptors, however, further investigation is needed to validate whether CD73 is specific for human rod photoreceptors (27,28) or might also mark photoreceptor precursors with the potential to differentiate into both, rods and cones (29). Contrary to FACS technology, MACS is routinely applicable in clinical settings, for example, for sorting of bone marrow cells prior transplantation (30).

Cellular mechanical properties, which might for example depend on the cell's actin cytoskeleton (31), have been proposed as a biomarker (32,33) for the identification of disease states (2,34), different cell populations (35–37), differentiation potential (3) as well as a basis for label-free cell separation (38,39). Morpho-rheological properties can be measured using a variety of methods such as atomic force microscopy (AFM), micropipette aspiration or optical stretchers, but these methods allow only low-throughput studies and are therefore time consuming and inefficient for larger scale analysis (33). Conversely, real-time deformability cytometry (RT-DC) represents a high-throughput, contactless microfluidic technique that measures rheological and morphological parameters such as size (by cross-sectional area), deformation and elasticity of single cells (40). In RT-DC, spherical cells are passing a constricted channel whereby they deform under hydrodynamic shear and normal stress. Cell parameters are acquired in real-time at rates approaching 1,000 cells per second allowing the analysis of large populations (>100,000 cells) with detailed statistics as example shown for identification of several cell-types in whole blood samples (36). Such high-throughput technology might be also important for the evaluation of heterogenous cell populations received from the dissociation of entire tissues like the retina, a part of the central nervous system that is composed of diverse neuronal cell types, that is, retinal ganglion cells, amacrines, bipolars, horizontals, rod and cone photoreceptors, besides glial cells including Müller cells, astrocytes, and microglial cells. While mechanical characterization of retinal tissue and some retinal cell types (amacrines, bipolars, and Müller glia) have been performed using different low-throughput methods (41–44), morpho-rheological properties of rod photoreceptors are currently unknown.

In this study, we use RT-DC assays for physical characterization of mouse rod photoreceptors at different stages during development. In comparison to other retinal cell types, rod photoreceptors displayed unique mechanical and morphological features, which are sufficient to discriminate them in a label-free manner. Additionally, we illustrate that mechanical properties of rod photoreceptors derived from mESC-retinal organoids follow the similar developmental trend as their in vivo counterparts. These results, therefore, identify basic parameters for high-throughput analysis and potential label-free sorting of rod photoreceptors for characterization and transplantation purposes.

Material & Methods

Isolation of Retinal Progenitor Cells and Rod Photoreceptors

Neural retina leucine zipper-enhanced green fluorescent protein (Nrl-eGFP) (45) and hairy and enhancer of split 5-GFP (Hes5-GFP) (46) mouse lines were used as a source for rods and retinal progenitor cells, respectively. Rod photoreceptors were isolated at embryonic day [E] 15.5 and at postnatal days [P] 4, 10, and 20 while retinal progenitor cells were harvested at E15.5 from time-mated breedings. At E15.5, pregnant females were euthanized using cervical dislocation, their abdomen cleaned with 70% ethanol (vol/vol) and the embryos were exposed using scissors. The placenta was isolated and transferred into a petri dish containing cold phosphate buffered saline (PBS). Eyes were dissected, the retinas isolated, transferred to a Papain solution (Worthington®, Lakewood, NY, USA) and incubated for 35 min at 37°C as previously described (21). Retinas were dissociated into a single cell suspension, spun down for 5 min at 300 rfc. Retinal cells were re-suspended in FACS buffer (2 mM ethylene diamine tetraacetic acid [EDTA] and 1% bovine serum albumin [BSA] in PBS) and passed through a 40 μm Nylon cell strainer (BD Biosciences, Heidelberg, Germany) before FAC-sorting. Mouse breedings, time-matings, and removal of embryos and organs were approved by the ethics committee of the TU Dresden and the Landesdirektion Dresden (approval number 24-9168.24-1/2007-27) and performed in accordance with the regulation of the European Union, German laws (Tierschutzgesetz), the ARVO statement for the Use of Animals in Ophthalmic and Vision Research, as well as the NIH Guide for the care and use of laboratory work.

Generation of mESC Derived Retinal Progenitor Cells and Rods

Wild-type E14TG2a and retinal homeobox protein—(Rx) GFP (4,47) mESCs were maintained in culture with their respective mESC maintenance culture medium (Supporting Information). On every media change or cell passage, mESC medium was

supplemented with 10^3U/ml leukemia inhibitory factor (LIF, Millipore, Schwalbach, Germany), 1 μM MEK inhibitor PD0325901 (Axon Medchem, Groningen, Netherlands) and Blasticidin (solely for Rx-GFP; 20 μg/ml; Thermo Scientific; R210-01, Schwerte, Germany). Cells were passaged every 3 days using TrypLE Express (Invitrogen, Schwerte, Germany).

Generation of retinal organoids using the mESC lines E14TG2a or Rx-GFP was performed as previously described (4,23). Briefly, 3,000 mESCs were seeded in 96-well U-bottomed, low adhesion plates (Nunclon Sphera Microplattes, Thermo Fisher, cat#174929, Schwerte, Germany) in their respective retinal differentiation medium (RDM), and 0.2% Matrigel (growth factor reduced, BD Biosciences, lot#5173009, Heidelberg, Germany) was added on on culture day (D) 1. Aggregates from E14TG2a mESC line were cultured at 37°C in normoxic conditions until D7, while Rx-GFP aggregates were cultured until D9 and further processed for FACS and RT-DC analysis. On D7, E14TG2a organoids were transferred to bacterial-grade petri dishes (Greiner Bio-One, Frickenhausen, Germany) and cultured in retinal maturation medium 1 (RMM1) at 37°C, 40% O_2. From D10 on, organoids were cultured in RMM2 at 37°C, 40% O_2; from D10 to D14 media was supplemented with 0.3 mM EC23 (Tocris Biosciences, cat# 4011, Bristol, UK). Fifty percent media exchanges (ME) were performed every 2–3 days, until transduction with AAV2/8YF Rho–green fluorescent protein (GFP) from D20 to D22. Hundred percent ME was performed on D22 to remove viral particles. Retinal organoids were kept in culture until D26.

Viral Vector Production

The pAAV2.1-ss-RHO-eGFP-WPRE cis plasmid was used to produce single-strand AAV8Y733F-pseudotyped AAV2 vectors (48) expressing eGFP under control of a human rhodopsin (RHO) promoter (49). The AAV vectors were purified from supernatants of transiently transfected HEK293T cells according to the method described by Becirovic and colleagues (50). Physical titers (in genome copies/ml) were determined by quantitative PCR on a StepOnePlus™ real-time PCR system (Applied Biosystems, Schwerte, Germany) using the assay described in by D'Costa et al. (51).

Fluorescent-Activated Cell Sorting

Retinal cells from primary tissue or mESC-derived origin were FAC-sorted using BD FACS Aria™ II with an 85 μm nozzle (BD Biosciences, Heidelberg, Germany). GFP-positive and GFP-negative fractions used for RT-DC were gated for life/death discrimination using propidium iodide (PI, BD Biosciences, Heidelberg, Germany), doublet discrimination, and sorted for the presence/absence of GFP.

Real-Time Deformability Cytometry

GFP-positive and negative FAC-sorted retinal cells were spun down for 5 min at 300 rfc and re-suspended in a measurement buffer (MB; see below) at a final concentration of 3×10^6 cells/ml, before analysis. Each sample was measured in RT-DC using a flow rate of 0.04 μl/s and chips with a 20 μm wide channel constriction. RT-DC is a microfluidics-based method that allows capturing of single cells in a deformed state (36). The general application, including analysis, has been described elsewhere (52). Briefly, using a syringe pump (NemeSyS, Cetoni, Korbussen, Germany), suspended cells are pumped through a microfluidic chip, which has a constriction with a slightly wider diameter than the cells. Starting with a cell suspension of 3×10^6 cells/ml and using a sample:sheathflow ratio of 1:3, the concentration within the measurement channel is 0.75×10^6 cells/ml or 750 cells/μl. With a flow rate of 0.04 μl/s a capture rate of 750 cells/μl * 0.04 μl/s = 30 cells/s was realized. The parabolic flow profile in the constriction causes shear and normal forces that deform the cells (maximum shear stress is approximately 4 kPa (53), which are recorded by a high-speed camera (EoSens CL MC1362, Mikrotron, Unterschleißheim, Germany).

For image acquisition and analysis, OpenCV 3.1 (http://opencv.org) and the ShapeIn (Zellmechanik Dresden GmbH) software were used. First, a background image was created by averaging the last 100 captured frames, which was subtracted from each successive image. Following threshold operations, a border-following algorithm (54) was used to determine the contour of the tracked object. The contour was used to calculate cell size by counting the pixels inside the contour and deformation (D) was derived from circularity (C) and is defined as following: $D = 1 - C = 1 - \frac{2\sqrt{\pi A}}{l}$ (l—perimeter of the contour, A—area of the contour). Deformation is zero for a perfect circle and smaller than one for an elongated object. In practice, the tracked contour is not smooth, but it has many small protrusions and spikes, which dramatically increases the perimeter. Therefore, the perimeter and area of a convex hull around the contour is used for calculating deformation. As large cells will get closer to the constriction wall, they will be subjected to higher shear forces than small cells. Therefore, the deformation is dependent on the size of cells. An analytical and numerical modeling (55,56) allows obtaining the elastic modulus for given deformation and area values. Elastic modulus is a physical property that can be used to quantify the stiffness of cells independently from their size. The shear and normal stress in the channel and, therefore, also the calculated elastic modulus, is depending on the viscosity of the measurement buffer (MB). MB was produced using PBS (without Mg^{2+}, Ca^{2+}) and methyl cellulose (4,000 cPs, Alfa Aesar, Kandel, Germany) to elevate the viscosity to 15 mPa (zero shear viscosity). The viscosity is underlying a shear thinning effect, which causes a decrease of the viscosity to approximately 10mPa for a flow rate of 0.04 μl/s in a 20 μm channel. These parameters have been used for the calculation of elastic modulus and plotted in iso-elasticity lines axis. The corresponding E values (kPa) of the plotted iso-elasticity lines are (from top (soft) to bottom (stiff)): 0.6, 0.8, 1.0, 1.2, 1.6, 2.0, 2.8, 3.6, 4.7 kPa.

The system provides real-time analysis of these parameters and results are therefore instantaneously available. A single experimental run typically lasts for 1–2 min, which, at a measurement rate of 30 cells/s, yields 1,800–3,600 cells measured in total.

Tissue Processing, Immunohisto- and Cytochemistry

Eyes from the Nrl-eGFP (45) and Hes5-GFP (46) mouse lines were collected at different developmental stages (embryonic day [E]15.5 and postnatal days [P] 4, 10, and 20) enucleated and transferred to a petri-dish containing cold PBS. Using a $30^{1/2}$ Gauge sharp needle (BD Micro-Lance™ 3, VWR, Dresden, Germany), a small hole was performed in the ora serrata and the eyes were transferred to a 4% Paraformaldehyde solution (PFA, Merck Millipore, Schwalbach, Germany) for 1 h at 4°C. The posterior segment of the eye was then isolated, cryopreserved overnight at 4°C in a 30% sucrose solution (weigh/volume, in PBS) and embedded in optimal cutting medium (OCT, NEG, Thermo Scientific, Schwerte, Germany). Rx-GFP and wild-type E14TG2a organoids were harvested at Day 9 and Day 26 of culture, respectively, fixed for 20 min at room temperature, cryopreserved, and embedded as mentioned above. Tissue and retinal organoids were cryo-sectioned (20 and 10 µm, respectively) and further processed for immunohistochemistry. Tissue sections were air-dried for 1 to 2 h, hydrated with PBS and blocked with blocking solution composed of 0.3% Triton-X (SERVA, Heidelberg, Germany), 5% donkey serum (DS) and 10% BSA (SERVA, Heidelberg, Germany). Primary antibodies (Table S2) were incubated overnight at 4°C. Slides were then washed three times for 10 min with PBS and incubated for 90 min at room temperature with the corresponding secondary antibodies conjugated with Cy2, Cy3, and Cy5 fluorophores (1:1,000, Jackson Immunoresearch, Cambridgeshire, UK) and 4′,6-diamidino-2-phenylindole (DAPI; 1:20,000; Sigma, Munich, Germany). Tissue sections were washed in PBS three times for 10 min and mounted with Aquapolymount (Polysciences, Heidelberg, Germany). For immunocytochemistry, undifferentiated mESCs were cultured in 1 cm diameter coverslips coated with poly-lysine. When undifferentiated mESC reached 80% confluence, cells were fixed with 4% PFA for 5 min at room temperature, rinsed with PBS and incubated in blocking solution. Primary (Table S2) and secondary antibodies used and time of incubations, washing steps and mounting were performed as described above for primary retinal tissue.

Image Acquisition and Processing

Images of immunofluorescent stainings were acquired using Apotome Imager Z1 (Zeiss, Jena, Germany) while retinal organoids were imaged using the inverted microscope Nikon Eclipse Ti (Nikon, Düsseldorf, Germany). Fiji and Adobe Illustrator (San Jose, CA, USA) were used to process all acquired images. All schemes and graphs were generated using Prims 6 and Adobe Illustrator (San Jose, CA, USA).

Statistical Analysis for RT-DC Data

Statistical analysis of acquired RT-DC data was performed as described in the Supporting Information.

Results

Postnatal Rods Have a Unique Mechanical Fingerprint Compared to Other Retinal Cells

Mechanical phenotyping has been proposed as a label-free method for cell characterization (38,39); however, distinct properties of rod photoreceptors have not been identified yet. Therefore, rod photoreceptors were isolated at different developmental stages (embryonic [E)] 15.5, postnatal day [P] 4, 10, and 20) from a previously established reporter mouse line, where the expression of eGFP is driven by the rod photoreceptor-specific Nrl promoter (Nrl-eGFP) (45) (Fig. S1). Nrl-eGFP retinas were dissociated to a single cell suspension and FAC-sorted based on reporter expression (Fig. 1). Both, GFP-positive (GFP^+) and GFP-negative (GFP^-) cell fractions were collected, re-suspended in RT-DC buffer, and analyzed by RT-DC (Fig. 1). RT-DC scatter plots from GFP^+ and GFP^- cell fractions displayed differential distribution patterns (Fig. 2a and Fig. S2). During retinal development, rod photoreceptors are significantly smaller in cell size (measured by cross-sectional area) compared to other retinal cells at all time points investigated (Table S1). However, no significant differences in deformation values and elastic modulus (Fig. 2b and Fig. S2, Table S1) were observed at E15.5. After birth, GFP^+ rods deformed significantly less and were more compliant (lower elastic modulus) in comparison to GFP^- cells (Table S1, Fig. 2b), which was a consistent trend throughout development. These results show that postnatal rod photoreceptors can be distinguished from any other retinal cell type by cell size, deformation, and elastic modulus.

Combinatorial Analysis of Cross Sectional Area, Elastic Modulus and Statistical Modeling Allows Improved Discrimination of Primary Rods from Other Cell Types

Despite the significant differences, especially in cross-sectional area between rods and other retinal cell types during postnatal development, the GFP^+ and GFP^- cell populations partially overlap as seen in the RT-DC scatter blots, independent of using highly pure FAC-sorted fractions (∼99%) (Fig. 2a and Fig. S2). The percentage of other cells that overlap with the rod cell population was calculated using the likelihood ratio of the two models, describing each data set (see Section 1) in area versus deformation space (AD) and area versus elastic modulus space (AE). In both scenarios, we observed an overlap of both cell populations ranging from ∼10% to ∼30%, depending on the developmental stage analyzed (area vs. deformation: E15.5: 21 ± 6.1, P4: 29.5 ± 1.7, P10: 9.1 ± 0.8, and P20: 17.7 ± 5.6; area vs. elastic modulus: E15.5: 16.7 ± 2.5%, P4: 28.1 ± 1.3, P10: 10.1 ± 1.1, and P20: 16.5 ± 5.03 in %; Fig. 3a). Since a smaller overlap allows better segregation of populations, especially area and elastic modulus are suited to separate GFP^+ and GFP^- cells. This result shows that the combination of size and elastic modulus allows an improved separation of rods (GFP^+) from other retinal cells (GFP^-) compared to any individual parameter alone. In spite of this combinatorial analysis, there is still an overlap of around 10% between the two populations,

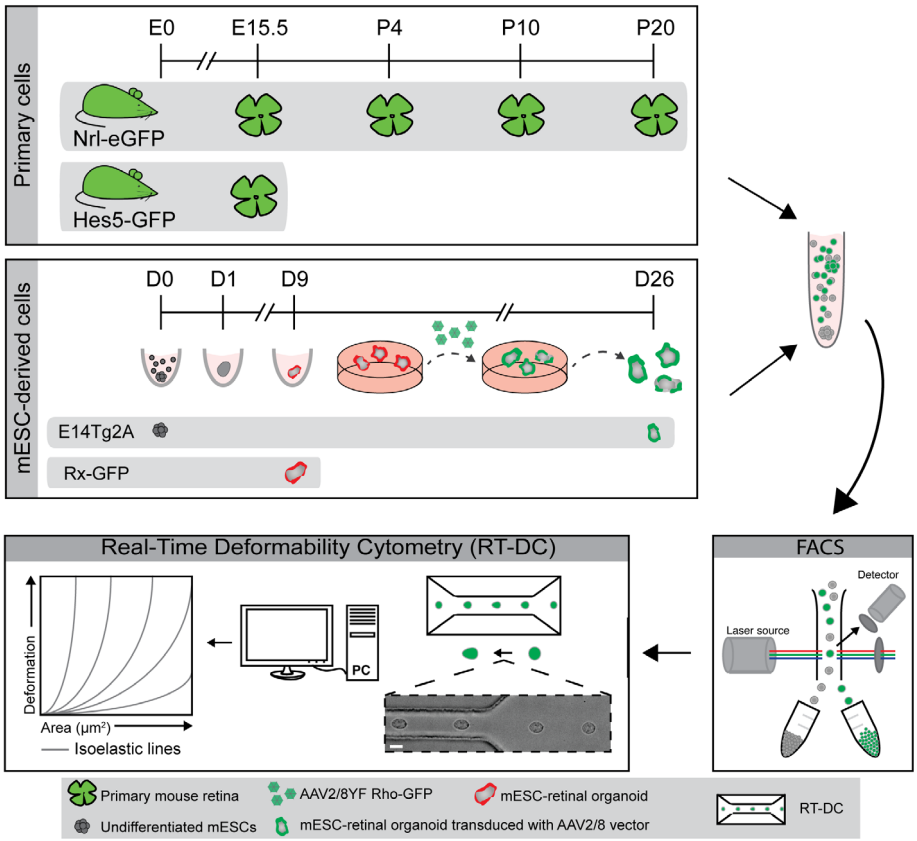

Figure 1. Graphical description of the experimental outline. Retinas from Nrl-eGFP (rod photoreceptor reporter) and Hes5-GFP (retinal progenitor cell reporter) mouse lines are dissociated to a single cell suspension, FAC-sorted for GFP^+ and GFP^- cell fractions and collected for real-time deformability cytometry (RT-DC) analysis at the selected developmental stages (embryonic day [E]15.5, postnatal day [P] 4, 10, and 20). Cell size (measured in cross-sectional area, μm^2), deformation and elastic modulus are acquired for individual cells and analyzed online. A similar approach is performed with mESC-derived retinal progenitor cells (mESC-Rx-GFP) at Day 9 of differentiation (D), and mESC (E14TG2a) derived rod photoreceptors at D26 labeled by AAV2/8 Rho-GFP. Analysis by RT-DC is performed in the same way as for primary cells. Scale bar: 5 µm.

suggesting the presence of other retinal cell types with similar mechanical properties like rods.

Following the identification of morpho-rheological parameters of developing rod photoreceptors, we determined whether these parameters could be used to prospectively identify rods in a heterogenous population such as the unsorted cell fraction of Nrl-eGFP retinae (Fig. S2, left column). A two-dimensional (2D) Gaussian mixture model (GMM) with $n = 2$ Gaussians was used wherein each cell was assigned to a cluster, representing either the GFP^+ or GFP^- fraction. The GMM provided mean values of both clusters for area ($[\mu_A] = \mu m^2$), deformation ($[\mu_D] = 1$) and elastic modulus ($[\mu_E] = kPa$). Area, deformation and elastic modulus values calculated by the 2D GMM for both clusters were sufficient to separate both subpopulations. They displayed similar trends as FAC-sorted GFP^+ and GFP^- primary data at all time-points analyzed. Interestingly, the values of elastic modulus (μ_E) for one cluster correctly matched the rod primary data (GFP^+) (E15.5: $0.9 \pm 3.5 \times 10^{-2}$; P4: $0.76 \pm 9 \times 10^{-3}$, P10: $0.84 \pm 1 \times 10^{-2}$, and P20: $0.85 \pm 7 \times 10^{-3}$ in kPa; Fig. S3). Predicted area (μ_A) and deformation (μ_D) values for the same cluster diverged slightly, but significantly, from the primary rod data (μ_A: E15.5: 49.9 ± 0.45, P4: 32.6 ± 0.11, P10: 25.66 ± 0.47, and P20: 25 ± 0.1 in μm^2; μ_D: E15.5: $0.04 \pm 2.7 \times 10^{-3}$, P4: $0.031 \pm 8.7 \times 10^{-4}$, P10: $0.02 \pm 7.7 \times 10^{-4}$, and P20: $0.019 \pm 2.8 \times 10^{-4}$). A similar trend was also observed for the second cluster which, theoretically, should correspond to the GFP^- population (μ_A: E15.5: 87.8 ± 2.68, P4: 49.04 ± 0.36, P10: 43.34 ± 0.87, and P20: 42.79 ± 0.73 in μm^2; μ_D: E15.5: $0.039 \pm 3.3 \times 10^{-3}$, P4: $0.027 \pm 6.17 \times 10^{-4}$, P10: $0.024 \pm 1.71 \times 10^{-3}$, and P20: $0.014 \pm 1.37 \times 10^{-4}$; μ_E: E15.5: $1.2 \pm 4.6 \times 10^{-2}$, P4: $1.02 \pm 1.2 \times 10^{-2}$, P10: $1.01 \pm 2.4 \times 10^{-2}$, and P20: $1.31 \pm 8.8 \times 10^{-3}$ in kPa; Fig. 3b and Fig. S3). These results suggest that rods can be distinguished from other retinal cells in an unlabeled heterogenous cell population, such as the retina, using morpho-rheological properties.

Embryonic Rods Are Mechanically Indistinguishable from Age-Matched Retinal Progenitor Cells

Rod photoreceptors represent a small cell population (3.63 ± 1.18%; mean ± *SD*, data not shown) at early embryonic stages (E15.5) in the developing mouse retina in contrast to retinal progenitor cells (66.2 ± 6.42%; mean ± *SD*, data not shown), based on the expression of Nrl-GFP and Hes5-GFP, respectively, and might have similar mechanical properties given that $Nrl\text{-}GFP^+$ cells are not significantly different to $Nrl\text{-}GFP^-$ in

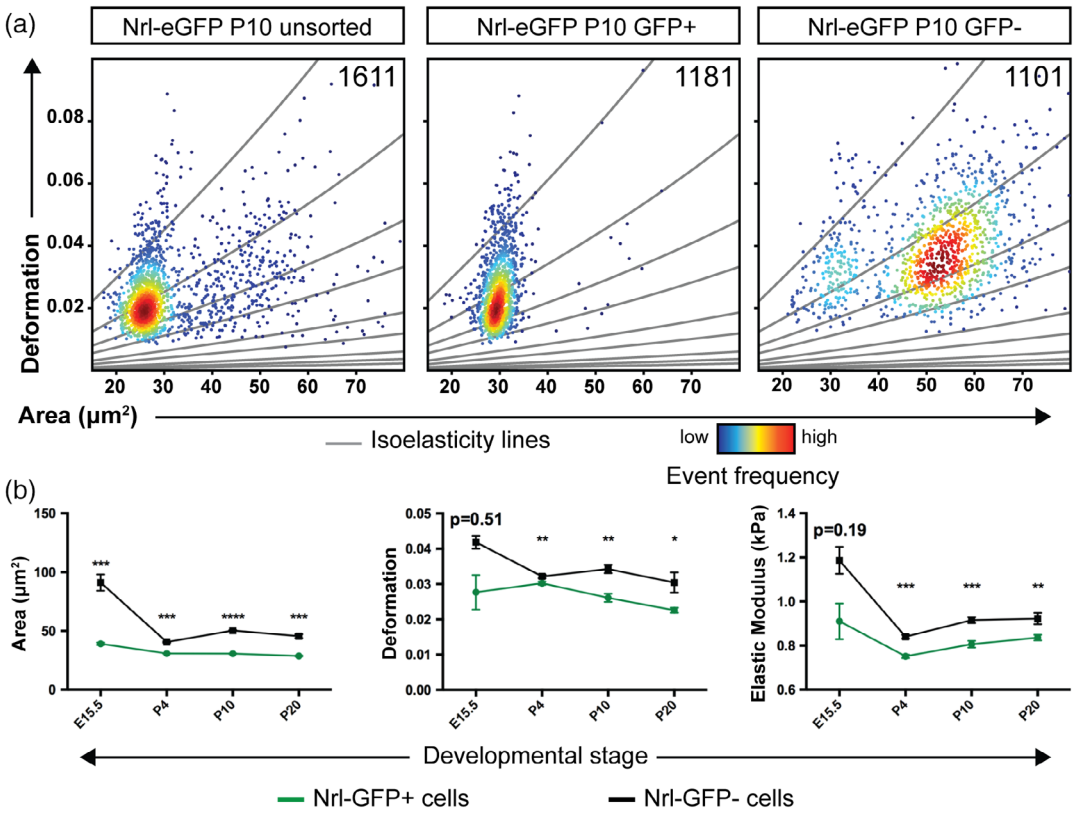

Figure 2. Rod photoreceptors acquire unique mechanical properties during retinal development. Rod photoreceptors from the Nrl-eGFP mouse line were isolated by FACS at different developmental stages (embryonic day [E] 15.5 and postnatal day [P] 4, 10, and 20) and analyzed for their mechanical properties by RT-DC. **(a)** Representative scatter plots of unsorted Nrl-eGFP retinae versus sorted Nrl-eGFP$^+$ and Nrl-eGFP$^-$ cells at P10. **(b)** during embryonic development, rods (Nrl-eGFP$^+$) differ from other retinal cell populations (Nrl-eGFP$^-$) mostly in cross sectional area (μm^2), whereas postnatal rods show significant differences in cross sectional area, deformation and elastic modulus, that is, they are smaller, deform less and are softer than age-matched Nrl-eGFP$^-$ cells (3 biological replicates analyzed). *N*: Number of cells; *P* value: * <0.05; ** <0.01; *** <0.001; **** <0.0001.

deformation values and elastic modulus when analyzed by RT-DC (Fig. 2b and Fig. S2, Table S1). To identify changes in mechanical properties of a retinal progenitor cell differentiating into a rod photoreceptor, retinal progenitor cells were separately analyzed. Therefore, retinal progenitors were isolated by FACS at E15.5 from a previously established reporter mouse line expressing GFP driven by the transcription factor hairy and enhancer of split 5 (Hes5-GFP; Fig. 1 and Fig. S1) (46). During embryonic development Hes5 is expressed in retinal progenitors and as development proceeds its expression becomes restricted to Müller glia cells (57). Analysis by RT-DC revealed that retinal progenitor cells (Hes5-GFP$^+$ fraction, Fig. 4a) were significantly larger and displayed a higher variability in area (Fig. 4a,b) than age-matched rods (Fig. S2 and Fig. 4b; Nrl-GFP$^+$ fraction). Conversely, no differences were observed in deformation and elasticity between these two cell types (Fig. 4b, Table S1), rendering rods (Nrl-eGFP$^+$) indistinguishable from Hes5-GFP$^+$ retinal progenitors at this early developmental stage. Additionally, scatter plots from Hes5-GFP$^+$ and age-matched Nrl-eGFP$^+$ fractions partially overlapped (18.02 $\pm$ 1.29%; Fig. 4c) and a combination of two parameters (area vs. deformation or area vs. elastic modulus) was not sufficient to discriminate Nrl-eGFP$^+$ rods from Hes5-GFP$^+$ retinal progenitors (Fig. 4d). This analysis confirms that rods are mechanically indistinguishable from retinal progenitors at E15.5. At this developmental stage, the mouse retina is composed of other cell types in addition to retinal progenitors such as rods, cones, amacrines, and ganglion cells (58) whose mechanical properties are yet unknown. Using 2D Gaussian mixture models and Bayesian information criterion (BIC) on the Hes5-GFP unsorted fraction, we estimated the number of clusters (subpopulations) present in AD as well as AE space. Interestingly, for both aforementioned spaces approximately three clusters were consistently found (average of three biological replicates: N_{AD} = 2.98 $\pm$ 0.08, N_{AE} = 2.81 $\pm$ 0.1). The contribution of a cluster to the total number of clusters was scaled according to its relative weight in the mixture. This suggests that mechanical properties can be used to distinguish other retinal cell types (Fig. S4).

mESC-Derived Rods Display Similar Morpho-Rheological Changes over Time as Primary Rods during Development

The derivation of photoreceptors from ESC/iPSC-derived retinal organoids is the current state-of-the-art method to produce high amounts of photoreceptors in vitro (4–7,9,11,14,23).

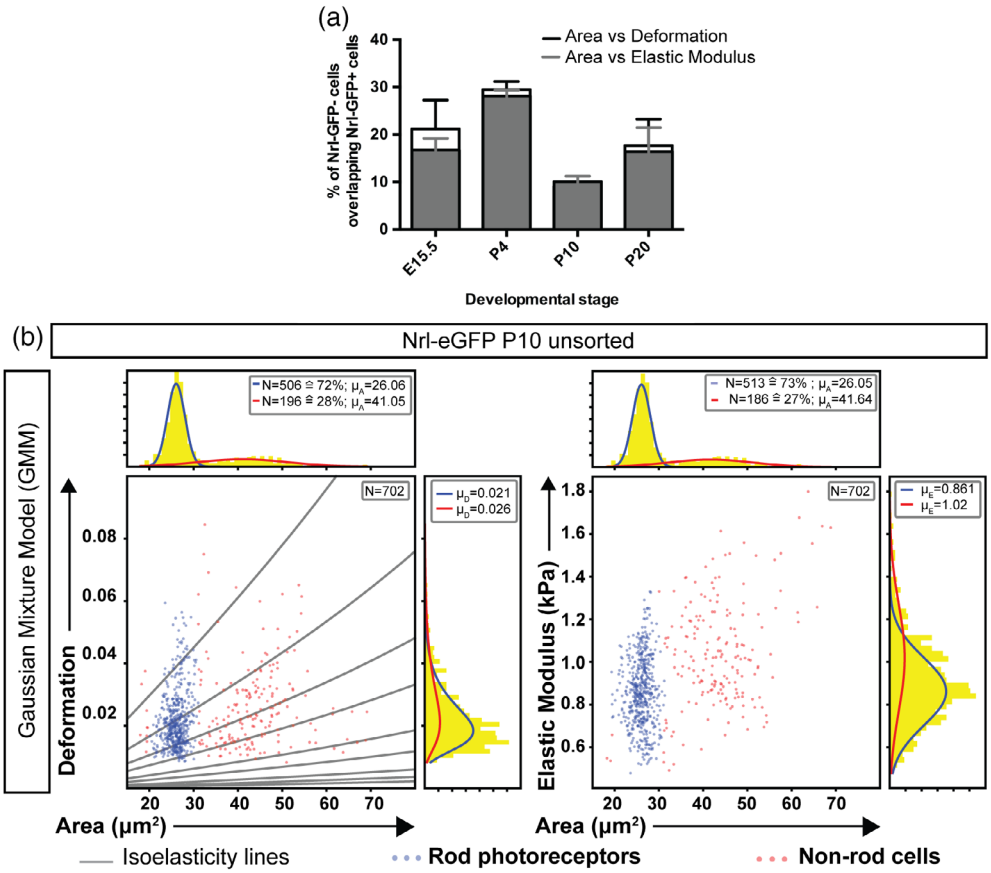

Figure 3. Prospective identification of rod photoreceptors within dissociated whole retinal tissue based on mixture models for elastic modulus and area. Probabilistic analysis of unsorted cell suspensions from Nrl-eGFP mice using mixture models and its comparative analysis to the primary cell data. **(a)** The Nrl-eGFP$^-$ cell population partially overlaps with rod photoreceptor population (Nrl-eGFP$^+$) in RT-DC analysis. Combined analysis of area versus elastic modulus leads to a slightly better, but not significant, separation between GFP$^+$ and GFP$^-$ populations compared to area versus deformation. **(b)** Representative scatter plot depicts two clusters (two subpopulations: Red corresponding to Nrl-eGFP$^-$ and blue corresponding to Nrl-eGFP$^+$) are assumed to predict the assignment of each event to one of the clusters in Nrl-eGFP P10 unsorted retinas using two dimensional (2D) Gaussian mixture models (GMM). Upper histograms show the overall distribution of the unsorted retinal cells (yellow bars) and the probabilistic distributions found by the mixture model (blue and red lines). Elastic modulus and deformation distributions are visualized in the same manner in the vertical histograms. *N*: number of cells; μ_A: mean area (μm^2); μ_D: mean deformation; μ_E: mean elastic modulus.

mESC-derived rod photoreceptors behave similarly as primary rods in transplantation settings (6). We hypothesized that the generation of mESC-derived rods display similar mechanical properties during development as their in vivo counterpart. Retinal organoids were generated from wild type (cell line E14TG2a) and a reporter mESC line expressing GFP under the control of the retina and anterior neural fold homeobox (Rax or Rx) promoter (Rx-GFP) (47). The wild type line was used to collect undifferentiated mESCs and mESC-derived rod photoreceptors, while the Rx-GFP line was used to generate sufficient amounts of retinal progenitor cells. In order to identify mESC-derived rods, retinal organoids were transduced from day of differentiation (D) 20 to D22 with adeno-associated virus AAV2/8YF harboring GFP under the control of the rhodopsin promoter (27). Undifferentiated mESCs were collected at D0, Rx-GFP$^+$ (retinal progenitor cells), and Rx-GFP$^-$ cells at D9, and mESC-derived rods were isolated at D26 (Figs. 1 and 5). Retinal progenitor cells and rods were FAC-sorted based on Rx-GFP and Rho-GFP expression, respectively, and all four different cell populations were analyzed using RT-DC. Interestingly, differentiation of rod photoreceptors from mESCs showed a continuous decrease in area (Fig. 6a) with a sharp decrease from an undifferentiated mESCs to a Rx-GFP$^+$ retinal progenitor state (Table S1). Retinal cells deformed less (undifferentiated mESCs: $0.048 \pm 2.7 \times 1^{-3}$; Rx-GFP$^+$ at D9: $0.037 \pm 7.8 \times 10^{-3}$; mESC-derived rods D26: $0.021 \pm 8.5 \times 10^{-4}$) and became more compliant as mESC differentiated toward the rod fate (elastic modulus; undifferentiated mESCs: $1.95 \pm 3.8 \times 10^{-2}$; Rx-GFP$^+$: $1.1 \pm 8.7 \times 10^{-2}$; mESC-derived rods D26: $0.94 \pm 3.4 \times 10^{-2}$ in kPa; Fig. 6a and Fig. S5, Table S1). Previous studies postulated that mESC-derived rods at D26 of differentiation were equivalent to primary rods at postnatal Day 4/5. This hypothesis was based on transcriptional data and similar transplantation outcomes using rods from both donor cell sources (6). At the morpho-rheological level, rods derived from postnatal Day 4 retinae and from mESCs following 26 days of differentiation were significantly different in area, deformation and elastic modulus (Fig. 6b,c and Fig. S5). Taken together, these results indicate that

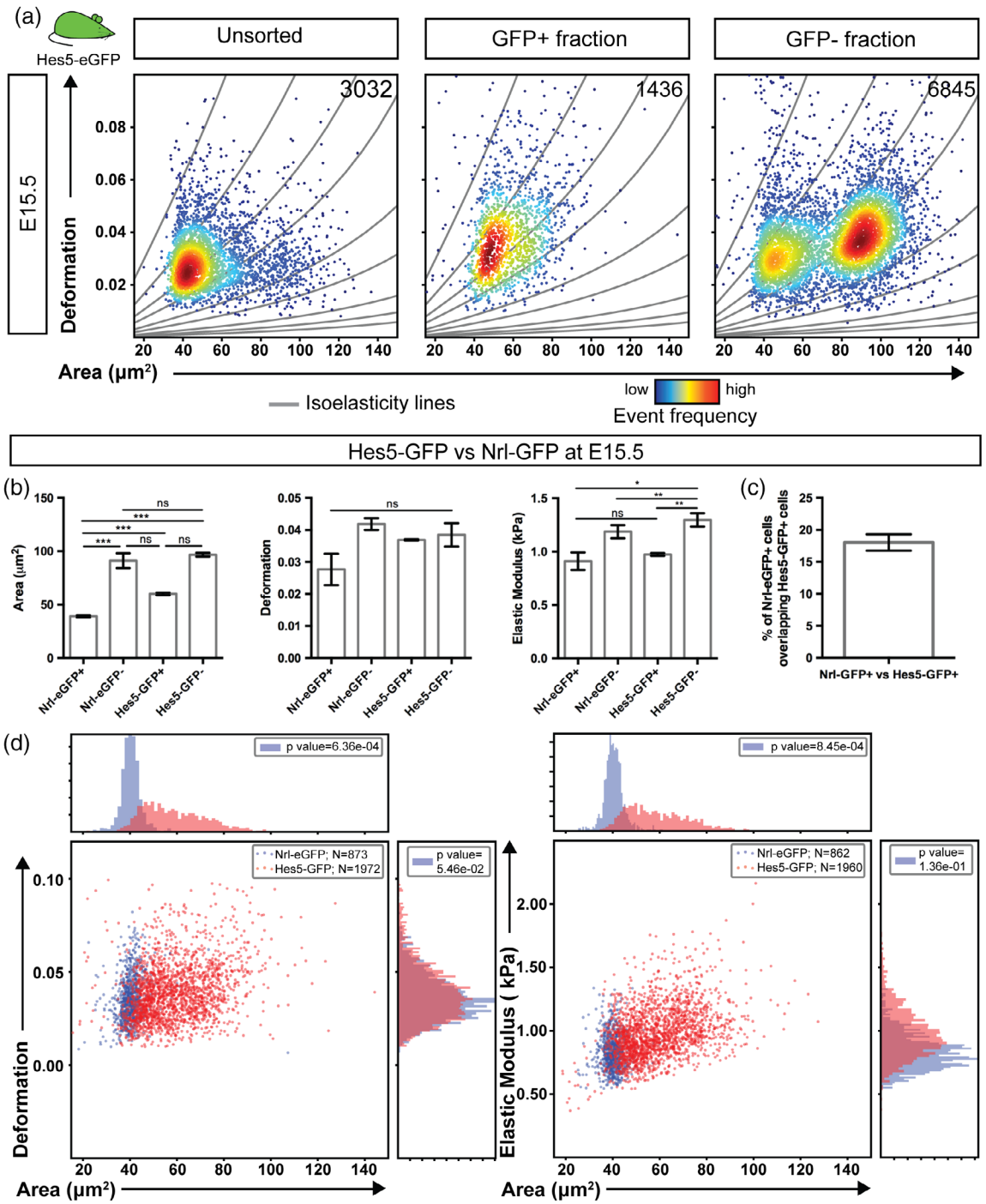

Figure 4. In early development rods show similar mechanical properties as retinal progenitor cells. **(a)** Scatter plot of unsorted Hes5-GFP retinal cells, Hes5-GFP-positive retinal progenitor cells (GFP$^+$ fraction) and Hes5-GFP-negative retinal cells (GFP$^-$ fraction) at embryonic day (E) 15.5. **(b)** Quantitative analysis of the measured parameters: Area (µm^2), deformation and elastic modulus and comparison with age-matched Nrl-eGFP$^+$ and Nrl-eGFP$^-$ cells (data from Fig. 2). At E15.5 Nrl-GFP$^+$ rods are smaller than Hes5-GFP$^+$ retinal progenitor cells but have similar deformation and elastic modulus values. **(c)** Quantification of the overlap between rod (Nrl-eGFP$^+$) and retinal progenitor (Hes5-GFP$^+$) distributions at E15.5. **(d)** Scatter plot comparing rods to retinal progenitor cells at E15.5: Individual analysis of each measured parameter shows no significant differences between both cell populations. *N*: number of cells; ns: not significant; *P* value: * <0.05; ** <0.01; *** <0.001.

mESC-derived rods show a similar trend in their mechanical properties during development as rods within the retina and that RT-DC might be a useful tool to add another level of characterization to phenotype rod photoreceptor maturation.

Discussion

In this study, we determined the morpho-rheological properties of primary and mESC-derived rod photoreceptors

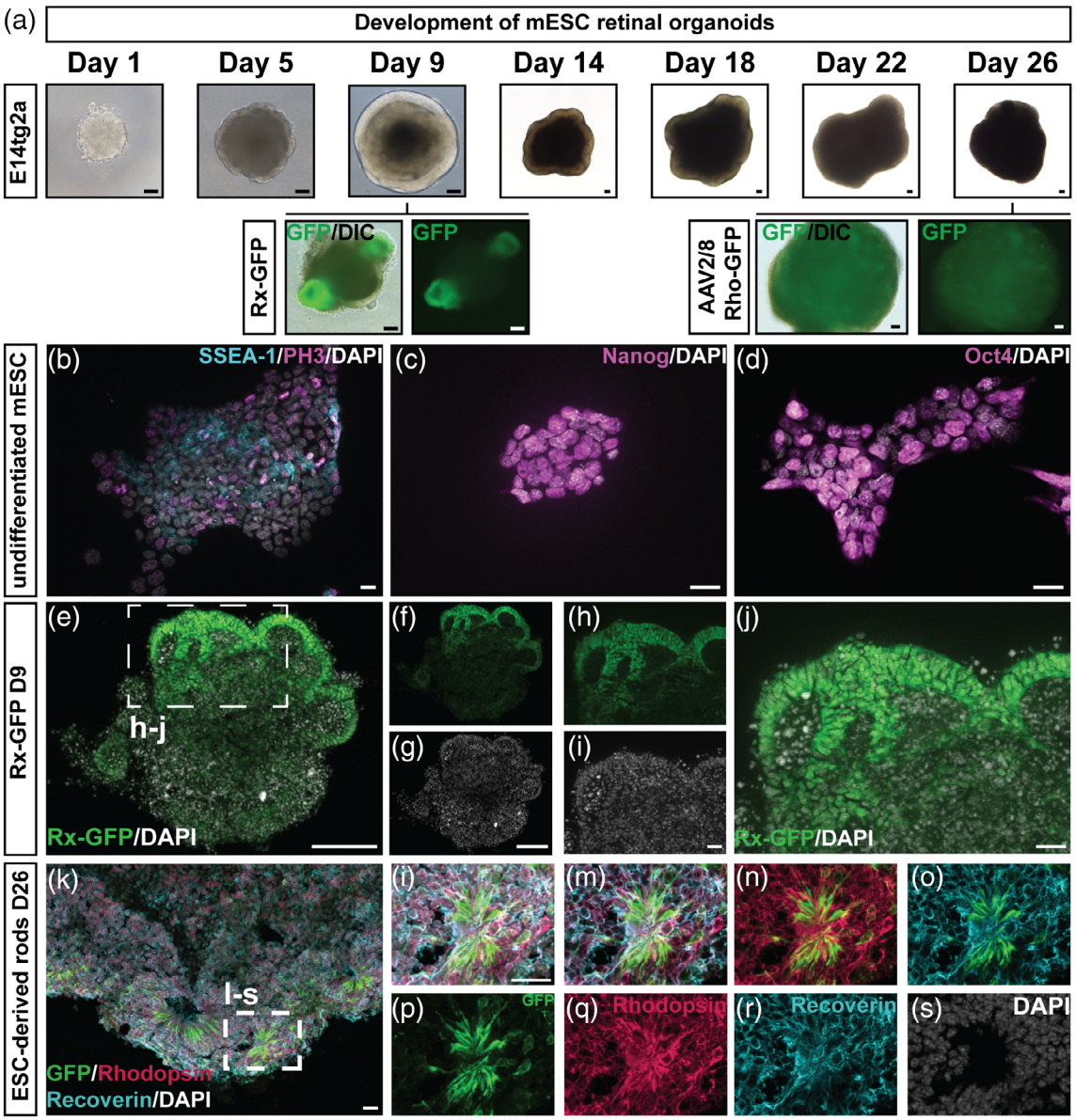

Figure 5. Generation of mESC-derived retinal organoids. **(a)** in vitro development of mouse embryonic stem cell (mESC)-derived retinal organoids using a wild-type line (E14TG2a) and the retinal progenitor reporter line Rx-GFP. Retinal progenitor cells were collected from Rx-GFP^{+} organoids at (D) 9 of differentiation while mESC-derived rods were harvested on D26 following viral transduction using AAV2/8 rho-GFP vector. **(b–d)** Undifferentiated mESC show positivity for the pluripotency markers SSEA-1 (cyan), Nanog (magenta) and Oct4 (magenta) as well as the cell cycle marker PH3 (magenta). **(e–j)** Rx-GFP mESC-organoids at D9 showed distinct GFP expression in epithelial-like structures. **(k–s)** At D26, E14TG2a mESC retinal organoids displayed high amounts of rod photoreceptors positive for rhodopsin (magenta) and recoverin (cyan), with some showing rod-specific viral GFP labelling (green). Nuclei were counterstained with DAPI (gray). Scale bar: (a), (e–g) 100 μm; (b–d) and (h–s): 20 μm.

during development. Our data indicates that RT-DC is a promising technology for retinal cell phenotyping and identification. RT-DC enables detection of differential developmental retinal cell changes and cell subtypes, specifically for prospective identification and label-free isolation of rod photoreceptors.

In the mouse postnatal retina, we observed an overall decrease in rod photoreceptor cell size, deformation and stiffness compared to embryonic developmental stages. This decrease in stiffness is in accordance with previous studies where postmitotic neurons (i.e., hippocampal neurons, amacrine, and bipolar retinal interneurons) isolated from the adult guinea pig or mouse CNS displayed low stiffness levels (41). During postnatal retinal development, retinal neurons project their processes and branch out in order to form the retinal neural circuitry. At this developmental stage retinal cells are more compliant than at embryonic stages (this study) and the low levels in stiffness might be required to promote axonal growth, branching and eventually neuronal maturation—developmental processes which have been correlated in vitro with soft substrates (59–61).

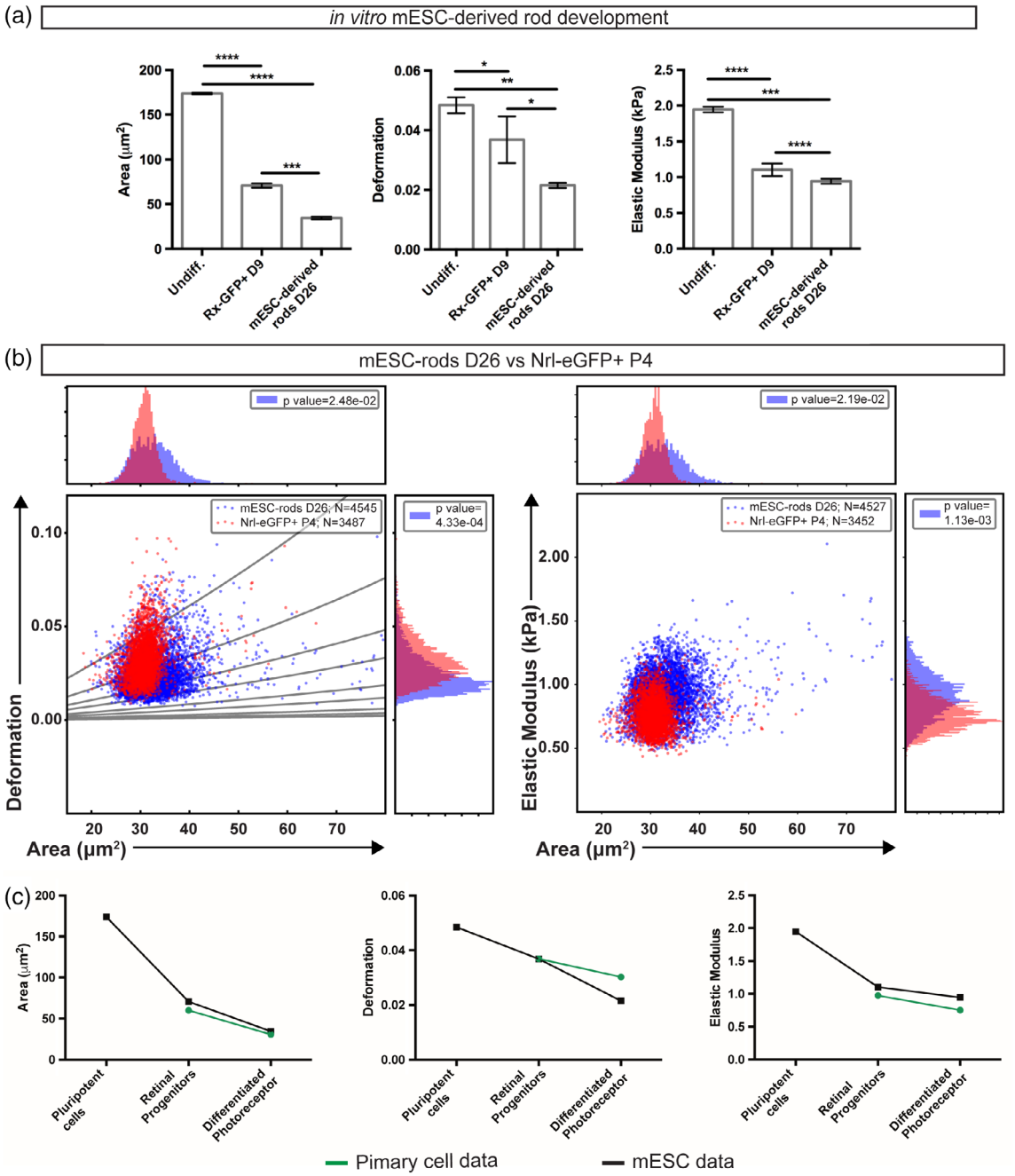

Figure 6. Over development mESC-derived rod photoreceptors show a similar morpho-rheological trend as primary rods. **(a)** Quantitative analysis of morpho-rheological properties of undifferentiated mESCs, mESC-Rx-GFP+ retinal progenitors at D9, and mESC-derived rods at D26 labeled with AAV2/8 Rho-GFP. All measured parameters, that is, area (µm^2), deformation and elastic modulus (kPa), displayed a significant decrease during differentiation and maturation. **(b)** Morpho-rheological properties of mESC-derived rods show significant differences compared to primary Nrl-eGFP+ rods at P4 (data from Fig. 2). **(c)** Comparison of mESC-derived rods with primary rods during development. Both rod populations displayed a similar overall trend with a constant decrease in area (µm^2), deformation and stiffness over time. *N*: Number of cells; *P* value: * <0.05; ** <0.01; *** <0.001; **** <0.0001.

Non-rod retinal cells (Nrl-GFP$^-$ population) showed increased stiffness compared to rods at all developmental stages. Non-photoreceptor cells are located in the inner nuclear and ganglion cell layer (INL and GCL, respectively) which also harbor the intra-retinal vasculature. Retinal angiogenesis occurs postnatally until the end of the third week and is restricted to the INL and GCL, leaving the photoreceptor layer avascular (62). Previous studies have suggested that the presence of stiffer substrates promotes blood vessel network formation, lumen formation, and vessel density, which would correlate with the higher stiffness of the Nrl-GFP$^-$ population compared to rods (63). On the other hand, the mechanical properties of the ONL, where in the mouse 98% of the cells are rod photoreceptors (64), might function as a barrier that limits blood vessel

growth into the ONL and therefore restricts angiogenesis to the retinal layers spanning the INL to GCL.

Although rods have unique mechanical properties during postnatal development, they still overlap with other cell types despite combined analysis of cross sectional area and elastic modulus. This suggests that other retinal cells share similar mechanical properties with rods. Separation of rods from other retinal cell types by morpho-rheological characteristics were modeled using two-dimensional (2D) Gaussian mixture models (GMM) in Nrl-eGFP unsorted samples at all developmental stages point to the presence of two clusters representing two distinct cell populations. Indeed, estimated values for area, deformation, and elasticity by the 2D GMM were sufficient to distinguish two cell populations. The elastic modulus for one cluster nicely matched with the rod photoreceptor population whereas area and deformation have a small, but significant difference to our FAC-sorted primary data. Differences between properties of the cluster and FAC-sorted cells could result from intrinsic differences in biological replicates, changes in the cells during the sorting procedure, slightly impure FAC-sorted fractions or an inaccurate assumption underlying the model (2D GMM assumes a Gaussian behavior of two clusters). Despite these differences, it was possible to mathematically identify a cluster of cells (subpopulation) in an unsorted retinal cell population where its rheological characteristics closely matched our FAC-sorted rod data. These results demonstrate the potential of mechanical properties for cell separation purposes from a heterogenous cell population such as the retina. Thus, further improvements in separating rods from other retinal cell-types are likely by adding further parameters that can be identified using machine learning/artificial intelligence (Ai) approaches.

In contrast to postnatal development, embryonic rods were indistinguishable from retinal progenitors at the mechanical level and combined analysis of Hes5-GFP unsorted and GFP^- fractions suggested the presence of at least three subpopulations at E15.5 (Fig. S4). We have used GMM and BIC to obtain an estimate of the number of clusters (subpopulations) in area versus deformation and area versus elastic modulus spaces. The contribution of each cluster to the total number of clusters was limited by its weight in order to avoid an overestimation (see Section 1), which resulted in the estimation of three clusters (subpopulations). Without weighting the contributions of small clusters, the total number of clusters was estimated to five, matching the assumed number of general cell-types at this developmental stage (i.e., ganglion cells, cone and rods photoreceptors, amacrines, and horizontal cells) (58). Therefore, we hypothesize, that each retinal cell type has a unique morpho-rheological signature, which can be predicted at early stages of development. However, such properties might be averaged as development proceeds due to physical cell packaging and organization in a stratified morphology (adult retina) and thus, the total number of clusters identified at this developmental stage reduced to three.

ESC/iPSC represents a virtually unlimited source for the generation of specific cell-types in vitro reducing the use of animals and circumventing the shortage of human material for research purposes. Particularly retinal organoid technology allows the generation of high amounts of photoreceptors within retina-like tissue structures that further contain the other main retinal cell-types besides some undefined cells (65). Interestingly, mESC-derived rod photoreceptors within organoids show a similar trend in their mechanical characteristics during development as primary rods in vivo: a decrease in cross sectional area, deformation, and stiffness. Undifferentiated mESCs were stiffer compared to cells committed to the retinal lineage, a feature that was also observed in other studies where mESCs were differentiated into other tissues and cell types (66–68). Unfortunately, a direct comparison between mESC-derived rods and other cell types present in the mESC retinal organoids, that is, GFP+ versus GFP^- fractions as it was performed for primary rods, could not be performed due to low AAV transduction efficiency ($3.63 \pm 2.96\%$ all of rod photoreceptors; mean $\pm$ *SD*) which is quite apart from the $\sim$60% of $CD73^+$ cells (cell surface marker for rods) present in these organoids at Day 26 of differentiation (23). However, taking into account the general developmental trend, we hypothesize that mESC-derived rods can be distinguished by mechanical properties from other cell-types present in mESC-retinal organoids. Interestingly, morpho-rheological properties of rods isolated from primary P4 retinas or from D26 mESC retinal organoids were slightly different. It might be that the developmental timing of cell and tissue maturation within organoids does not exactly match the in vivo development, either due to cell intrinsic processes or lack of other cellular components (e.g., vessels, microglia) that are missing in the organoid system. Moreover, the environmental differences between a living embryo/pup and a 3D cell culture system might be responsible for the deviation in mechanical properties of in vivo and in vitro generated rods as retinal organoids lack the physical constraints (e.g., lenses, surrounding mesenchymal tissue, orbital bones, or intra-ocular pressure) that are present during mouse development. Given the possibility of generating retinal organoids also from human ESC/iPSC, it will be of high interest to analyze also the morpho-rheological phenotype of human photoreceptors in future studies.

While the mechanical properties of photoreceptors at the single cell level has not been analyzed before, first studies assessed the physical constrains of mouse and porcine ocular tissues (69) or of the nuclear and plexiform layers within the retina (70). Thus, due to its neural composition the retina displayed a significantly lower compressive modulus than that of the sclera or cornea (69), while the nuclear layers and particularly the outer nuclear layer that is highly packed with photoreceptor cell bodies is the stiffest region within the retina (70). Interestingly, in retinal degenerative mice (C3H/HeJPde6rd1), with significant loss of photoreceptors from 3 weeks of age, the mean modulus at 12 weeks was reduced by more than 90% compared to the wild type C57BL6 mouse at a similar age (69). While the underlying cause for these differences have still to be analyzed in more detail, it shows that mechanical properties might have important influence on disease progression and should be considered as a potential new route for disease phenotyping in retinal degeneration. Furthermore, such

mechanical properties should be considered in designing photoreceptor transplantation approaches in the retina, including the stiffness of supporting polymer scaffolds, as first studies suggest that survival, maturation and axonal outgrowth of neurons is influenced by the stiffness of the recipient tissue (69).

The unique physical properties identified for photoreceptors might represent the bases for a novel label-free sorting approach for their isolation from heterogenous tissues like primary retinas or pluripotent stem cell-derived retinal organoids, as it will circumvent the timely and cost intensive generation of genetic engineered reporter cells. This will be of particular interest in regard to the isolation of rod or cone photoreceptors for clinical application in future cell transplantation approaches for treating degenerative retinal diseases (71).

By using RT-DC, we showed for the first time that rod photoreceptors have unique biomechanical characteristics distinguishing them from other retinal cell types and allowing their prospective label-free isolation. In principle, these findings could be exploited using passive sorting devices sensitive to particle size and stiffness, such as deterministic-lateral displacement or microfluidic forces (38,39,72). In these, the sorting properties have to be known a priori and instruct the device design and geometry, which are then fixed. In contrast, RT-DC is suggesting an active sorting alternative, where gating properties can be selected arbitrarily due to the real-time analysis—once the down-stream sorting is established. Recently, an active cell sorter has been introduced (73), which can also utilize a bright field image to determine when a sorting signal should be triggered. Sorting is facilitated using piezoelectrically actuated glass-membrane pumps. Alternatively, active cell sorting might be facilitated by using surface acoustic waves (74). The distinct mechanical properties identified for rod photoreceptors during development might be considered as additional parameters affecting retinal cell differentiation, tissue formation, disease progression or cell therapy approaches and should be taken into account in future studies.

Acknowledgments

We like to thank Sabrina Richter and Kathrin Sippel for animal husbandry, Drs. Anand Swaroop and Sandra Cottet for providing Nrl-eGFP mice and Dr. Verdon Taylor (University of Basel) for sharing the Hes5-GFP mouse line. The Rx-GFP-mESC line was provided by the RIKEN BioResource Center (RIKEN BRC) through the National Bio-Resource Project of the MEXT, Japan. We thank Dr. Yoshiki Sasai (RIKEN, Japan) for the Rx-GFP K/I EB5 line. E14TG2a mESC line was kindly provided by Dr. Konstantinos Anastassiadis, BIOTEC, Technische Universität Dresden. This work was supported by the Flow Cytometry Facility and the Microstructure Facility, both core facilities of BIOTEC/CRTD at Technische Universität Dresden, which are in part funded by the European Fund for Regional Development (EFRE) and the State of Saxony. This work was financially supported by the Deutsche Forschungsgemeinschaft (DGF) FZT 111, Center for Regenerative Therapies Dresden, EXC68 Cluster of Excellence (M.A.), DFG Grants AD375/3-1, SPP2127 GU612/5-1 (J.G.), KA 2794/5-1 (M.O.K.), AD375/7-1 (M.A.), the Bundesministerium für Bildung und Forschung (ZIK HIKE grant to O.O.), the Alexander von Humboldt Stiftung (Alexander von Humboldt Professorship to J.G.), the DZNE (M.O.K) and HGF Ex-Net0007 (M. O.K), and the ProRetina Stiftung (M.A.).

Conflict of Interests

Oliver Otto is co-founder and CSO of Zellmechanik Dresden, a company distributing the RT-DC technology.

Literature Cited

1. Furukawa T, Hurley JB, Kawamura S, editors. Vertebrate Photoreceptors—Functional Molecular Bases. Japan: Springer, 2014.
2. Guck J, Schinkinger S, Lincoln B, Wottawah F, Ebert S, Romeyke M, Lenz D, Erickson HM, Ananthakrishnan R, Mitchell D, et al. Optical deformability as an inherent cell marker for testing malignant transformation and metastatic competence. Biophys J 2005;88:3689–3698.
3. Gonzalez-Cruz RD, Fonseca VC, Darling EM. Cellular mechanical properties reflect the differentiation potential of adipose-derived mesenchymal stem cells. Proc Natl Acad Sci 2012;109:E1523–E1529.
4. Eiraku M, Takata N, Ishibashi H, Kawada M, Sakakura E, Okuda S, Sekiguchi K, Adachi T, Sasai Y. Self-organizing optic-cup morphogenesis in three-dimensional culture. Nature 2011;472:51–56.
5. Nakano T, Ando S, Takata N, Kawada M, Muguruma K, Sekiguchi K, Saito K, Yonemura S, Eiraku M, Sasai Y. Self-formation of optic cups and storable stratified neural retina from human ESCs. Cell Stem Cell 2012;10:771–785.
6. Gonzalez-Cordero A, West EL, Pearson RA, Duran Y, Carvalho LS, Chu CJ, Naeem A, Blackford SJI, Georgiadis A, Lakowski J, et al. Photoreceptor precursors derived from three-dimensional embryonic stem cell cultures integrate and mature within adult degenerate retina. Nat Biotechnol 2013;31:741–747.
7. Decembrini S, Koch U, Radtke F, Moulin A, Arsenijevic Y. Derivation of traceable and transplantable photoreceptors from mouse embryonic stem cells. Stem Cell Rep 2014;2:853–865.
8. Kaewkhaw R, Kaya KD, Brooks M, Homma K, Zou J, Chaitankar V, Rao M, Swaroop A. Transcriptome dynamics of developing photoreceptors in three-dimensional retina cultures recapitulates temporal sequence of human cone and rod differentiation revealing cell surface markers and gene networks. Stem Cells 2015;33:3504–3518.
9. Völkner M, Zschätzsch M, Rostovskaya M, Overall RW, Busskamp V, Anastassiadis K, Karl MO. Retinal Organoids from pluripotent stem cells efficiently recapitulate Retinogenesis. Stem Cell Rep 2016;6:525–538.
10. Lamba DA, McUsic A, Hirata RK, Wang PR, Russell D, Reh TA. Generation, purification and transplantation of photoreceptors derived from human induced pluripotent stem cells. PLoS One 2010;5:e8763.
11. Meyer JS, Howden SE, Wallace KA, Verhoeven AD, Wright LS, Capowski EE, Pinilla I, Martin JM, Tian S, Stewart R, et al. Optic vesicle-like structures derived from human pluripotent stem cells facilitate a customized approach to retinal disease treatment. Stem Cells 2011;29:1206–1218.
12. Tucker BA, Mullins RF, Streb LM, Anfinson K, Eyestone ME, Kaalberg E, Riker MJ, Drack AV, Braun TA, Stone EM. Patient-specific iPSC-derived photoreceptor precursor cells as a means to investigate retinitis pigmentosa. Elife 2013;2:e00824.
13. Phillips MJ, Perez ET, Martin JM, Reshel ST, Wallace KA, Capowski EE, Singh R, Wright LS, Clark EM, Barney PM, et al. Modeling human retinal development with patient-specific induced pluripotent stem cells reveals multiple roles for visual system Homeobox 2. Stem Cells 2014;32:1480–1492.
14. Zhong X, Gutierrez C, Xue T, Hampton C, Vergara MN, Cao LH, Peters A, Park TS, Zambidis ET, Meyer JS, et al. Generation of three-dimensional retinal tissue with functional photoreceptors from human iPSCs. Nat Commun 2014;5:4047.
15. MacLaren RE, Pearson RA, MacNeil A, Douglas RH, Salt TE, Akimoto M, Swaroop A, Sowden JC, Ali RR. Retinal repair by transplantation of photoreceptor precursors. Nature 2006;444:203–207.
16. Pearson RA, Barber AC, Rizzi M, Hippert C, Xue T, West EL, Duran Y, Smith AJ, Chuang JZ, Azam SA, et al. Restoration of vision after transplantation of photoreceptors. Nature 2012;485:99–103.
17. Barber AC, Hippert C, Duran Y, West EL, Bainbridge JWB, Warre-Cornish K, Luhmann UFO, Lakowski J, Sowden JC, Ali RR, et al. Repair of the degenerate retina by photoreceptor transplantation. Proc Natl Acad Sci 2013;110:354–359.
18. Lakowski J, Han Y-T, Pearson RA, Gonzalez-Cordero A, West EL, Gualdoni S, Barber AC, Hubank M, Ali RR, Sowdena JC. Effective transplantation of photoreceptor precursor cells selected via cell surface antigen expression. Stem Cells 2011;29:1391–1404.
19. Balse E, Tessier LH, Fuchs C´, Forster V´, Sahel J´A, Picaud S. Purification of mammalian cone photoreceptors by Lectin Panning and the enhancement of their survival in glia-conditioned medium. Invest Ophthalmol Vis Sci 2005;46:367–374.
20. Singh MS, Charbel Issa P, Butler R, Martin C, Lipinski DM, Sekaran S, Barnard AR, MacLaren RE. Reversal of end-stage retinal degeneration and

restoration of visual function by photoreceptor transplantation. Proc Natl Acad Sci 2013;110:1101–1106.

21. Santos-Ferreira T, Postel K, Stutzki H, Kurth T, Zeck G, Ader M. Daylight vision repair by cell transplantation. Stem Cells 2015;33:79–90.
22. Eberle D, Schubert S, Postel K, Corbeil D, Ader M. Increased integration of transplanted CD73-positive photoreceptor precursors into adult mouse retina. Invest Opthal Vis Sci 2011;52:6462.
23. Santos-Ferreira T, Völkner M, Borsch O, Haas J, Cimalla P, Vasudevan P, Carmeliet P, Corbeil D, Michalakis S, Koch E, et al. Stem cell-derived photoreceptor transplants differentially integrate into mouse models of cone-rod dystrophy. Invest Opthal Vis Sci 2016;57:3509.
24. Eberle D, Santos-Ferreira T, Grahl S, Ader M. Subretinal transplantation of MACS purified photoreceptor precursor cells into the adult mouse retina. J Vis Exp 2014; 84:e50932.
25. Koso H, Minami C, Tabata Y, Inoue M, Sasaki E, Satoh S, Watanabe S. CD73, a novel cell surface antigen that characterizes retinal photoreceptor precursor cells. Invest Opthal Vis Sci 2009;50:5411.
26. Lakowski J, Gonzalez-Cordero A, West EL, Han YT, Welby E, Naeem A, Blackford SJI, Bainbridge JWB, Pearson RA, Ali RR, et al. Transplantation of photoreceptor precursors isolated via a cell surface biomarker panel from embryonic stem cell-derived self-forming retina. Stem Cell 2015;33:2469–2482.
27. Reichman S, Slembrouck A, Gagliardi G, Chaffiol A, Terray A, Nanteau C, Potey A, Belle M, Rabesandratana O, Duebel J, et al. Generation of storable retinal organoids and retinal pigmented epithelium from adherent human iPS cells in Xeno-free and feeder-free conditions. Stem Cells 2017;35:1176–1188.
28. Lakowski J, Welby E, Budinger D, di Marco F, di Foggia V, Bainbridge JWB, Wallace K, Gamm DM, Ali RR, Sowden JC. Isolation of human photoreceptor precursors via a cell surface marker panel from stem cell-derived retinal organoids and fetal retinae. Stem Cells 2018;36:709–722.
29. Gagliardi G, Ben M'Barek K, Chaffiol A, Slembrouck-Brec A, Conart JB, Nanteau C, Rabesandratana O, Sahel JA, Duebel J, Orieux G, et al. Characterization and transplantation of CD73-positive photoreceptors isolated from human iPSC-derived retinal Organoids. Stem Cell Rep 2018;11:665–680.
30. Richel DJ, Johnsen HE, Canon J, Guillaume T, Schaafsma MR, Schenkeveld C, Hansen SW, McNiece I, Gringeri AJ, Briddell R, et al. Highly purified CD34+ cells isolated using magnetically activated cell selection provide rapid engraftment following high-dose chemotherapy in breast cancer patients. Bone Marrow Transplant 2000;25:243–249.
31. Lautenschläger F, Paschke S, Schinkinger S, Bruel A, Beil M, Guck J. The regulatory role of cell mechanics for migration of differentiating myeloid cells. Proc Natl Acad Sci 2009;106:15696–15701.
32. Elson EL. Cellular mechanics as an indicator of cytoskeletal structure and function. Annu Rev Biophys Biophys Chem 1988;17:397–430.
33. Carlo DD. A mechanical biomarker of cell state in medicine. J Lab Autom 2012;17: 32–42.
34. Tse HTK, Gossett DR, Moon YS, Masaeli M, Sohsman M, Ying Y, Mislick K, Adams RP, Rao J, di Carlo D. Quantitative diagnosis of malignant pleural effusions by single-cell mechanophenotyping. Sci Transl Med 2013;5:212ra163–212ra163.
35. Darling EM, Topel M, Zauscher S, Vail TP, Guilak F. Viscoelastic properties of human mesenchymally-derived stem cells and primary osteoblasts, chondrocytes, and adipocytes. J Biomech 2008;41:454–464.
36. Otto O, Rosendahl P, Mietke A, Golfier S, Herold C, Klaue D, Girardo S, Pagliara S, Ekpenyong A, Jacobi A, et al. Real-time deformability cytometry: On-the-fly cell mechanical phenotyping. Nat Methods 2015;12:199–202.
37. Xavier M, Rosendahl P, Herbig M, Kräter M, Spencer D, Bornhäuser M, Oreffo ROC, Morgan H, Guck J, Otto O. Mechanical phenotyping of primary human skeletal stem cells in heterogeneous populations by real-time deformability cytometry. Integr Biol 2016;8:616–623.
38. Gossett DR, Weaver WM, Mach AJ, Hur SC, Tse HT, Lee W, Amini H, di Carlo D. Label-free cell separation and sorting in microfluidic systems. Anal Bioanal Chem 2010;397:3249–3267.
39. Beech JP, Holm SH, Adolfsson K, Tegenfeldt JO. Sorting cells by size, shape and deformability. Lab Chip 2012;12:1048–1051.
40. Urbanska M, Rosendahl P, Kräter M, Guck J. High-throughput single-cell mechanical phenotyping with real-time deformability cytometry. Methods Cell Biol 2018; 175-198(2018):147.
41. Lu Y-B, Franze K, Seifert G, Steinhauser C, Kirchhoff F, Wolburg H, Guck J, Janmey P, Wei EQ, Kas J, et al. Viscoelastic properties of individual glial cells and neurons in the CNS. Proc Natl Acad Sci 2006;103:17759–17764.
42. Franze K, Francke M, Günter K, Christ AF, Körber N, Reichenbach A, Guck J. Spatial mapping of the mechanical properties of the living retina using scanning force microscopy. Soft Matter 2011;7:3147–3154.
43. Lu Y-B, Iandiev I, Hollborn M, Körber N, Ulbricht E, Hirrlinger PG, Pannicke T, Wei EQ, Bringmann A, Wolburg H, et al. Reactive glial cells: Increased stiffness correlates with increased intermediate filament expression. FASEB J 2011;25:624–631.
44. Lu Y-B, Pannicke T, Wei EQ, Bringmann A, Wiedemann P, Habermann G, Buse E, Käs JA, Reichenbach A. Biomechanical properties of retinal glial cells: Comparative and developmental data. Exp Eye Res 2013;113:60–65.
45. Akimoto M, Cheng H, Zhu D, Brzezinski JA, Khanna R, Filippova E, Oh ECT, Jing Y, Linares JL, Brooks M, et al. Targeting of GFP to newborn rods by Nrl promoter and temporal expression profiling of flow-sorted photoreceptors. Proc Natl Acad Sci USA 2006;103:3890–3895.
46. Basak O, Taylor V. Identification of self-replicating multipotent progenitors in the embryonic nervous system by high notch activity and Hes5 expression. Eur J Neurosci 2007;25:1006–1022.
47. Wataya T, Ando S, Muguruma K, Ikeda H, Watanabe K, Eiraku M, Kawada M, Takahashi J, Hashimoto N, Sasai Y. Minimization of exogenous signals in ES cell culture induces rostral hypothalamic differentiation. Proc Natl Acad Sci 2008;105: 11796–11801.
48. Koch S, Sothilingam V, Garcia Garrido M, Tanimoto N, Becirovic E, Koch F, Seide C, Beck SC, Seeliger MW, Biel M, et al. Gene therapy restores vision and delays degeneration in the CNGB1$^{-/-}$ mouse model of retinitis pigmentosa. Hum Mol Genet 2012;21:4486–4496.
49. Allocca M, Mussolino C, Garcia-Hoyos M, Sanges D, Iodice C, Petrillo M, Vandenberghe LH, Wilson JM, Marigo V, Surace EM, et al. Novel adeno-associated virus serotypes efficiently transduce murine photoreceptors. J Virol 2007;81: 11372–11380.
50. Becirovic E, Böhm S, Nguyen ONP, Riedmayr LM, Hammelmann V, Schön C, Butz ES, Wahl-Schott C, Biel M, Michalakis S. AAV vectors for FRET-based analysis of protein-protein interactions in photoreceptor outer segments. Front Neurosci 2016;10(356):1–13.
51. D'Costa S, Blouin V, Broucque F, Penaud-Budloo M, Fçranois A, Perez IC, le Bec C, Moullier P, Snyder RO, Ayuso E. Practical utilization of recombinant AAV vector reference standards: Focus on vector genomes titration by free ITR qPCR. Mol Ther Methods Clin Dev 2016;3:16019.
52. Herbig M, Kräter M, Plak K, Müller P, Guck J, Otto O. Real-time deformability cytometry: Label free functional characterization of cells. Flow Cytometry Protocols. New York: Springer, 2018.
53. Mietke A, Otto O, Girardo S, Rosendahl P, Taubenberger A, Golfier S, Ulbricht E, Aland S, Guck J, Fischer-Friedrich E. Extracting cell stiffness from real-time deformability cytometry: Theory and experiment. Biophys J 2015;109: 2023–2036.
54. Suzuki S, Abe K. Topological structural analysis of digitized binary images by border following. Comp Vis Graph Image Process 1985;30:32–46.
55. Mokbel M, Mokbel D, Mietke A, Träber N, Girardo S, Otto O, Guck J, Aland S. Numerical simulation of real-time deformability cytometry to extract cell mechanical properties. ACS Biomater Sci Eng 2017;3:2962–2973.
56. Herold C. Mapping of deformation to apparent Young's modulus in real-time deformability cytometry. arXiv, USA, 2017.
57. Nelson BR, Ueki Y, Reardon S, Karl MO, Georgi S, Hartman BH, Lamba DA, Reh TA. Genome-wide analysis of Müller glial differentiation reveals a requirement for notch signaling in postmitotic cells to maintain the glial fate. PLoS One 2011;6: e22817.
58. Marquardt T, Gruss P. Generating neuronal diversity in the retina: One for nearly all. Trends Neurosci 2002;25:32–38.
59. Georges PC, Miller WJ, Meaney DF, Sawyer ES, Janmey PA. Matrices with compliance comparable to that of brain tissue select neuronal over glial growth in mixed cortical cultures. Biophys J 2006;90:3012–3018.
60. Flanagan LA, Ju Y-E, Marg B, Osterfield M, Janmey PA. Neurite branching on deformable substrates. Neuroreport 2002;13:2411–2415.
61. Teixeira AI, Ilkhanizadeh S, Wigenius JA, Duckworth JK, Inganäs O, Hermanson O. The promotion of neuronal maturation on soft substrates. Biomaterials 2009;30: 4567–4572.
62. Stahl A, Connor KM, Sapieha P, Chen J, Dennison RJ, Krah NM, Seaward MR, Willett KL, Aderman CM, Guerin KI, et al. The mouse retina as an angiogenesis model. Invest Ophthalmol Vis Sci 2010;51:2813–2826.
63. LaValley DJ, Reinhart-King CA. Matrix stiffening in the formation of blood vessels. Adv Regen Biol 2014;1:25247.
64. Jeon CJ, Strettoi E, Masland RH. The major cell populations of the mouse retina. J Neurosci 1998;18:8936–8946.
65. Llonch S, Carido M, Ader M. Organoid technology for retinal repair. Dev Biol 2018; 433:132–143.
66. Bongiorno T, Kazlow J, Mezencev R, Griffiths S, Olivares-Navarrete R, McDonald JF, Schwartz Z, Boyan BD, McDevitt TC, Sulchek T. Mechanical stiffness as an improved single-cell indicator of osteoblastic human mesenchymal stem cell differentiation. J Biomech 2014;47:2197–2204.
67. Ekpenyong AE, Whyte G, Chalut K, Pagliara S, Lautenschläger F, Fiddler C, Paschke S, Keyser UF, Chilvers ER, Guck J. Viscoelastic properties of differentiating blood cells are fate- and function-dependent. PLoS One 2012;7:e45237.
68. Chowdhury F, Na S, Li D, Poh YC, Tanaka TS, Wang F, Wang N. Material properties of the cell dictate stress-induced spreading and differentiation in embryonic stem cells. Nat Mater 2010;9:82–88.
69. Worthington KS, Wiley LA, Bartlett AM, Stone EM, Mullins RF, Salem AK, Guymon CA, Tucker BA. Mechanical properties of murine and porcine ocular tissues in compression. Exp Eye Res 2014;121:194–199.
70. Weber IP, Yun SH, Scarcelli G, Franze K. The role of cell body density in ruminant retina mechanics assessed by atomic force and Brillouin microscopy. Phys Biol 2017;14(6):065006.
71. Gasparini S, Llonch S, Borsch O, Ader M. Transplantation of photoreceptors into the degenerative retina: Current state and future perspectives. Prog Retin Eye Res 2019;69:1–37.
72. Holmes D, Whyte G, Bailey J, Vergara-Irigaray N, Ekpenyong A, Guck J, Duke T. Separation of blood cells with differing deformability using deterministic lateral displacement. Interface Focus 2014;4:20140011–20140011.
73. Nitta N, Sugimura T, Isozaki A, Mikami H, Hiraki K, Sakuma S, Iino T, Arai F, Endo T, Fujiwaki Y, et al. Intelligent image-activated cell sorting. Cell 2018;175:266–276.
74. Nawaz AA, Chen Y, Nama N, Nissly RH, Ren L, Ozcelik A, Wang L, McCoy JP, Levine SJ, Huang TJ. Acoustofluidic fluorescence activated cell sorter. Anal Chem 2015;87(24):12051–12058.